

Spacecraft State Estimation

AE4313: Spacecraft Attitude Dynamics and Control

Richard Adam



Introduction

This report presents the design, implementation, and evaluation of a nonlinear state estimation method, specifically an EKF, for a spacecraft with a simple PD controller. The objective is to create a simple attitude controller and compare the performance of the spacecraft under ideal sensor measurements, noisy sensor measurements without state estimation, and noisy sensor measurements with an Extended Kalman Filter applied for state estimation.

The spacecraft follows a circular orbit at an altitude of 700km. It is actively controlled along all three rotational axes with no limitations on the control torques available, although the controller is designed to have a maximum torque around 5-6Nm, which hydrazine attitude control thrusters can achieve. Its moments of inertia are given by the diagonal inertia matrix:

$$\mathbf{J} = \begin{bmatrix} J_{11} & 0 & 0 \\ 0 & J_{22} & 0 \\ 0 & 0 & J_{33} \end{bmatrix} = \begin{bmatrix} 2700 & 0 & 0 \\ 0 & 2300 & 0 \\ 0 & 0 & 3000 \end{bmatrix} \text{ kg} \cdot \text{m}^2$$

The spacecraft is subjected to constant disturbance torques of $\mathbf{T}_d = [0.001, 0.001, 0.001]^T$ Nm about its body-fixed x, y, and z axes respectively. The reference attitude is fixed at zero roll, pitch, and yaw, and the system must maintain an attitude tracking accuracy within 0.1° for each axis. The initial attitude deviation from this reference is significant, with initial roll, pitch, and yaw errors of 5.0° .

Attitude information is provided by sun and earth horizon sensors, which directly measure roll, pitch, and yaw angles. The sun and earth horizon sensors have a gaussian white-normal noise with standard deviation σ_{w_i} applied to their measurements. The angular rate information is provided by a rate gyroscope on each body-fixed axis, all of which have an associated bias b_i . The σ_{w_i} and b_i for each sensor measurement can be seen in Table 1:

Attitude Angle	θ_1	θ_2	θ_3
Noise	$\sigma_{w_1} = 0.1^\circ$	$\sigma_{w_2} = 0.1^\circ$	$\sigma_{w_3} = 0.1^\circ$
Angular Rate	ω_1	ω_2	ω_3
Bias	$b_1 = 0.1^\circ/\text{s}$	$b_2 = -0.1^\circ/\text{s}$	$b_3 = 0.15^\circ/\text{s}$

Table 1: Noise and Bias For all Spacecraft Sensors

The design process for the system follows several steps. The first step is to derive the nonlinear equations of motion(EOMs) of the spacecraft and define it's coordinate system. After the equations of motion are derived, a simple PD controller is designed and simulated with ideal sensor measurements. Next, the realistic noise for the spacecraft sensors is integrated with the control system and the response is simulated again to measure the effect of noise on a spacecraft with no state estimation. Finally, an extended Kalman filter(EKF) is designed and integrated into the noisy control system for state estimation, and again the response is simulated and compared with the previous two responses. The EKF is designed to estimate the bias of the gyros, so the effectiveness of the gyro bias estimation is evaluated. In addition, a statistical analysis is done on EKF effectiveness across two different initialization conditions to evaluate how the attitude response changes.

Spacecraft EOM Derivation

Coordinate Frame Definition

The first step in determining the dynamics of the spacecraft is to define the coordinate systems. Due to the nature of spacecraft sensors, there are two important coordinate systems to note: spacecraft orbital frame and spacecraft body frame. The spacecraft orbital frame can be seen as a projection onto the orbital plane in Figure 1a, where x_o is in the direction of the orbit, y_o is perpendicular to the orbital plane(going into the page in Fig 1a) and z_o is "nadir-pointing", or pointing toward Earth's center. The body frame, on the other hand, is shown in Figure 1b, using the cube to represent the spacecraft itself. Both the orbital and body frames have the origin at the spacecraft center of mass.

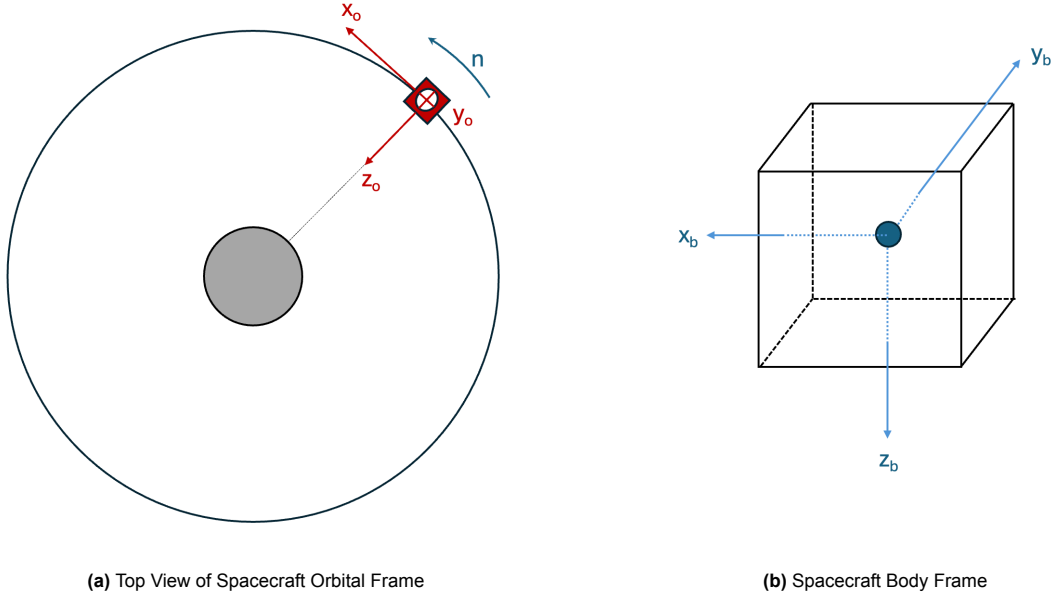


Figure 1: Spacecraft Reference Frames

These frames lead into the definition of attitude angles for the spacecraft. θ_1 , θ_2 , and θ_3 are the Euler angles roll, pitch, and yaw, respectively. These are defined as the angles by which, starting with the orbital and body frames aligned, you can rotate the body frame by θ_1 in x_b , then by θ_2 in y_b , then by θ_3 in z_b to achieve a given spacecraft attitude. The rotation matrix representing the transformation from orbital to body frame is given by:

$${}^o_C = \begin{bmatrix} \cos \theta_2 \cos \theta_3 & \cos \theta_2 \sin \theta_3 & -\sin \theta_2 \\ \sin \theta_1 \sin \theta_2 \cos \theta_3 - \cos \theta_1 \sin \theta_3 & \sin \theta_1 \sin \theta_2 \sin \theta_3 + \cos \theta_1 \cos \theta_3 & \sin \theta_1 \cos \theta_2 \\ \cos \theta_1 \sin \theta_2 \cos \theta_3 + \sin \theta_1 \sin \theta_3 & \cos \theta_1 \sin \theta_2 \sin \theta_3 - \sin \theta_1 \cos \theta_3 & \cos \theta_1 \cos \theta_2 \end{bmatrix}$$

Spacecraft attitude angles are measured in the orbital frame, but angular rates and control torques are respectively measured and applied in the body frame. Inertial sensors like gyroscopes provide body-fixed measurements while actuators like control moment gyros provide body-fixed control actions. The rates ω_1 , ω_2 , and ω_3 are defined as the instantaneous angular rates about x_b , y_b , and z_b respectively, while the control moments $M_{c,x}$, $M_{c,y}$, and $M_{c,z}$ and disturbance torques $M_{d,x}$, $M_{d,y}$, and $M_{d,z}$ are both in the body frame as well.

Dynamics and Kinematics Equations

The spacecraft under examination is a nadir-pointing satellite in a circular orbit at 700 km altitude. The equations governing its motion are derived from Euler's rotational dynamics and kinematics. The state vector x comprises the roll, pitch, and yaw angles ($\theta_1, \theta_2, \theta_3$) and corresponding angular rates ($\omega_1, \omega_2, \omega_3$).

To form the kinematic equations, one can start with the equation:

$$\bar{\omega}^{b/i} = \bar{\omega}^{b/o} + \bar{\omega}^{o/i}$$

Where $\bar{\omega}^{b/i}$ is the total body-fixed angular velocity, $\bar{\omega}^{b/o}$ is the velocity of the body frame with respect to the orbital frame, and $\bar{\omega}^{o/i}$ is the velocity of the orbital frame with respect to the Earth-Centered Earth-Fixed frame. $\bar{\omega}^{b/o}$ and $\bar{\omega}^{o/i}$ can be expressed as:

$$\bar{\omega}^{b/o} = \begin{bmatrix} 1 & 0 & -\sin \theta_2 \\ 0 & \cos \theta_1 & \sin \theta_1 \cos \theta_2 \\ 0 & -\sin \theta_1 & \cos \theta_1 \cos \theta_2 \end{bmatrix} \begin{bmatrix} \theta_1 \\ \theta_2 \\ \theta_3 \end{bmatrix}, \quad \bar{\omega}^{o/i} = -n \begin{bmatrix} \cos \theta_2 \sin \theta_3 \\ \sin \theta_1 \sin \theta_2 \sin \theta_3 + \cos \theta_1 \cos \theta_3 \\ \cos \theta_1 \sin \theta_2 \sin \theta_3 - \sin \theta_1 \cos \theta_3 \end{bmatrix}$$

Combining these equations, the expression for $\bar{\omega}^{b/i}$ is:

$$\begin{bmatrix} \dot{\theta}_1 \\ \dot{\theta}_2 \\ \dot{\theta}_3 \end{bmatrix} = \begin{bmatrix} 1 & 0 & -\sin \theta_2 \\ 0 & \cos \theta_1 & \sin \theta_1 \cos \theta_2 \\ 0 & -\sin \theta_1 & \cos \theta_1 \cos \theta_2 \end{bmatrix} \begin{bmatrix} \dot{\theta}_1 \\ \dot{\theta}_2 \\ \dot{\theta}_3 \end{bmatrix} - n \begin{bmatrix} \cos \theta_2 \sin \theta_3 \\ \sin \theta_1 \sin \theta_2 \sin \theta_3 + \cos \theta_1 \cos \theta_3 \\ \cos \theta_1 \sin \theta_2 \sin \theta_3 - \sin \theta_1 \cos \theta_3 \end{bmatrix}$$

Inverting this expression for $\dot{\theta}$, one obtains the expression:

$$\begin{bmatrix} \dot{\theta}_1 \\ \dot{\theta}_2 \\ \dot{\theta}_3 \end{bmatrix} = \frac{1}{\cos \theta_2} \begin{bmatrix} \cos \theta_2 & \sin \theta_1 \sin \theta_2 & \cos \theta_1 \sin \theta_2 \\ 0 & \cos \theta_1 \cos \theta_2 & -\sin \theta_1 \cos \theta_2 \\ 0 & \sin \theta_1 & \cos \theta_1 \end{bmatrix} \begin{bmatrix} \omega_1 \\ \omega_2 \\ \omega_3 \end{bmatrix} + \frac{n}{\cos \theta_2} \begin{bmatrix} \sin \theta_3 \\ \cos \theta_2 \cos \theta_3 \\ \sin \theta_2 \sin \theta_3 \end{bmatrix}$$

This expression can be simplified by assuming that the effect of n and θ_3 are small over the course of a single control action, nullifying the second part of the expression and leading to the final kinematic expression:

$$\begin{aligned} \dot{\theta}_1 &= \omega_1 + (\omega_2 \sin \theta_1 + \omega_3 \cos \theta_1) \tan \theta_2 \\ \dot{\theta}_2 &= \omega_2 \cos \theta_1 - \omega_3 \sin \theta_1 \\ \dot{\theta}_3 &= \frac{\omega_2 \sin \theta_1 + \omega_3 \cos \theta_1}{\cos \theta_2} \end{aligned}$$

The dynamic equations incorporating the gravitational gradient torque and external disturbance torques are derived from the Euler Equation:

$$J \cdot \dot{\omega} + \bar{\omega} \times J \bar{\omega} = \sum M$$

plugging in gravitational torques, disturbance torques M_d , and control torques M_c , one obtains the matrix equation:

$$\begin{aligned} & \begin{bmatrix} J_{11} & J_{12} & J_{13} \\ J_{21} & J_{22} & J_{23} \\ J_{31} & J_{32} & J_{33} \end{bmatrix} \begin{bmatrix} \dot{\omega}_1 \\ \dot{\omega}_2 \\ \dot{\omega}_3 \end{bmatrix} + \begin{bmatrix} 0 & -\omega_3 & \omega_2 \\ \omega_3 & 0 & -\omega_1 \\ -\omega_2 & \omega_1 & 0 \end{bmatrix} \begin{bmatrix} J_{11} & J_{12} & J_{13} \\ J_{21} & J_{22} & J_{23} \\ J_{31} & J_{32} & J_{33} \end{bmatrix} \begin{bmatrix} \omega_1 \\ \omega_2 \\ \omega_3 \end{bmatrix} \\ &= 3n^2 \begin{bmatrix} 0 & -C_{33} & C_{23} \\ C_{33} & 0 & -C_{13} \\ -C_{23} & C_{13} & 0 \end{bmatrix} \begin{bmatrix} J_{11} & J_{12} & J_{13} \\ J_{21} & J_{22} & J_{23} \\ J_{31} & J_{32} & J_{33} \end{bmatrix} \begin{bmatrix} C_{13} \\ C_{23} \\ C_{33} \end{bmatrix} + \begin{bmatrix} M_{d,x} \\ M_{d,y} \\ M_{d,z} \end{bmatrix} + \begin{bmatrix} M_{c,x} \\ M_{c,y} \\ M_{c,z} \end{bmatrix} \end{aligned}$$

where n is the orbital rate. Solving this expression for the $\dot{\omega}$ terms results in the dynamics equations:

$$\begin{aligned} \dot{\omega}_1 &= \frac{M_{a_1} + M_{d1} - (J_{33} - J_{22})\omega_2\omega_3 - 3n(J_{33} - J_{22})\cos \theta_1 \sin \theta_1 \cos^2 \theta_2}{J_{11}} \\ \dot{\omega}_2 &= \frac{M_{a_2} + M_{d2} - (J_{11} - J_{33})\omega_1\omega_3 - 3n(J_{33} - J_{11})\cos \theta_1 \cos \theta_2 \sin \theta_2}{J_{22}} \\ \dot{\omega}_3 &= \frac{M_{a_3} + M_{d3} - (J_{22} - J_{11})\omega_1\omega_2 + 3n(J_{11} - J_{22})\sin \theta_1 \sin \theta_2 \cos \theta_2}{J_{33}} \end{aligned}$$

The state matrix is $x = [\theta_1, \theta_2, \theta_3, \omega_1, \omega_2, \omega_3]^T$. Thus, the full expression $\dot{x} = f(x, u)$ can be expressed as:

$$\dot{x} = \begin{bmatrix} \dot{\theta}_1 \\ \dot{\theta}_2 \\ \dot{\theta}_3 \\ \dot{\omega}_1 \\ \dot{\omega}_2 \\ \dot{\omega}_3 \end{bmatrix} = \begin{bmatrix} \omega_1 + (\omega_2 \sin \theta_1 + \omega_3 \cos \theta_1) \tan \theta_2 \\ \omega_2 \cos \theta_1 - \omega_3 \sin \theta_1 \\ \frac{\omega_2 \sin \theta_1 + \omega_3 \cos \theta_1}{\cos \theta_2} \\ \frac{M_{a_1} + M_{d1} - (J_{33} - J_{22})\omega_2\omega_3 - 3n(J_{33} - J_{22}) \cos \theta_1 \sin \theta_1 \cos^2 \theta_2}{J_{11}} \\ \frac{M_{a_2} + M_{d2} - (J_{11} - J_{33})\omega_1\omega_3 - 3n(J_{33} - J_{11}) \cos \theta_1 \cos \theta_2 \sin \theta_2}{J_{22}} \\ \frac{M_{a_3} + M_{d3} - (J_{22} - J_{11})\omega_1\omega_2 + 3n(J_{11} - J_{22}) \sin \theta_1 \sin \theta_2 \cos \theta_2}{J_{33}} \end{bmatrix}$$

Controller Design and Ideal Sensor Simulation

A PD controller was implemented for each attitude axis. The controller computes torques using the PD equation:

$$\mathbf{M}_c = K_p \boldsymbol{\theta} + K_d \boldsymbol{\omega}$$

The gains were manually tuned to achieve a maximum control torque of about 5Nm, which is realistic for hydrazine attitude control thrusters, though somewhat high for a medium-sized spacecraft. For the interested reader, control torque graphs can be seen in the attached Jupyter Notebook file. The final gains were chosen to be:

$$K_p = \text{diag}(-50, -50, -50), \quad K_d = \text{diag}(-750, -750, -750)$$

The closed-loop system was simulated using the dynamics equation and the simple Euler integration routine $x_{k+1} = x_k + f(x_k, u_k)\Delta t$ where Δt is a constant timestep and $f(x_k, u_k)$ is the system dynamics function from the previous section evaluated at the current state with the current control action M_c .

The system was first simulated using ideal sensor conditions, meaning there is no sensor noise or bias. The results of the simulation can be seen in Figure 2:

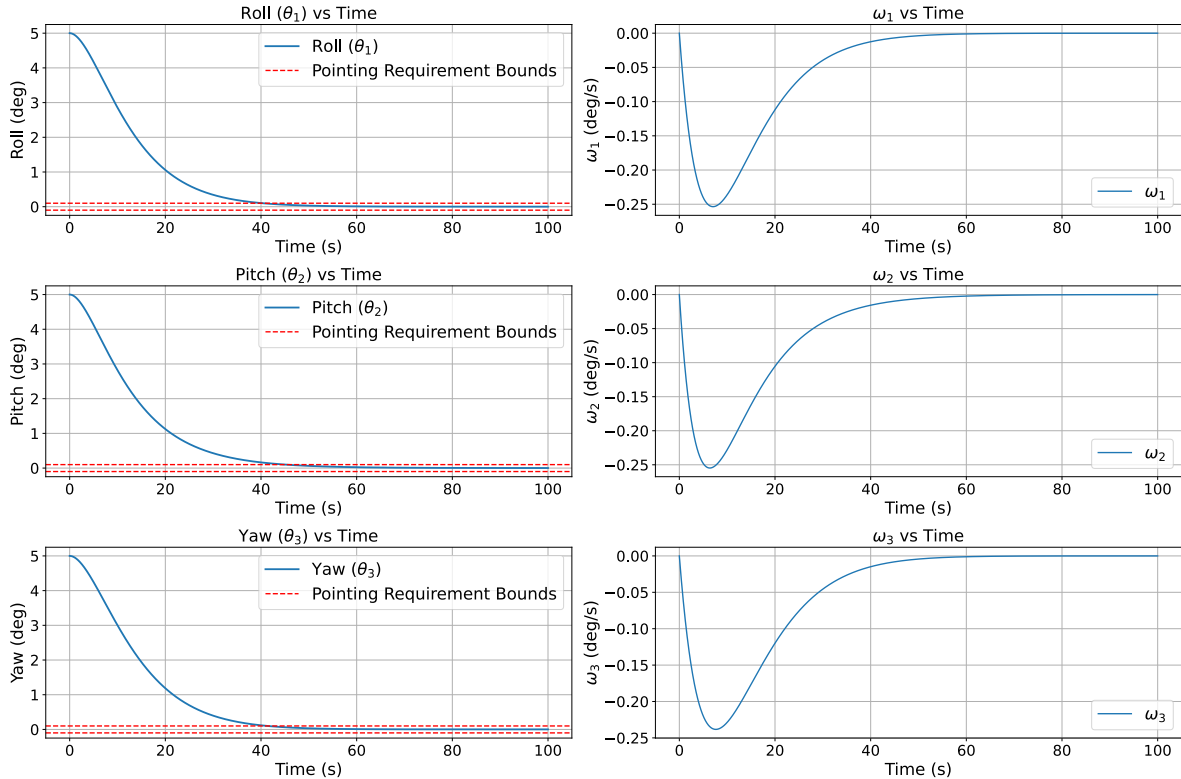


Figure 2: Attitude and Rate Response using ideal sensors (no bias or noise)

Clearly, with ideal sensors and a PD controller, the spacecraft converges to the within the target bounds after about 40 seconds.

Simulation with Noise and Bias

After the ideal sensor simulation, the system was simulated with realistic sensor noise added. Gyro bias and attitude noise were included, but no gyro noise is included, so the equation for measured states, or the observation equation, is:

$$x_{meas} = \begin{bmatrix} \theta_{1,meas} \\ \theta_{2,meas} \\ \theta_{3,meas} \\ \omega_{1,meas} \\ \omega_{2,meas} \\ \omega_{3,meas} \end{bmatrix} = h(x) + v(t) = \begin{bmatrix} \theta_1 \\ \theta_2 \\ \theta_3 \\ \omega_1 + b_1 \\ \omega_2 + b_2 \\ \omega_3 + b_3 \end{bmatrix} + \begin{bmatrix} w_1 \\ w_2 \\ w_3 \\ 0 \\ 0 \\ 0 \end{bmatrix} \quad (1)$$

Where w_1, w_2, w_3 are mutually uncorrelated white noise and b_1, b_2, b_3 are constant gyro biases, both of whose characteristics can be seen in Table 1. The control action in this case is dependent on flawed measurements from the sensors, and the result can be seen in Figure 3:

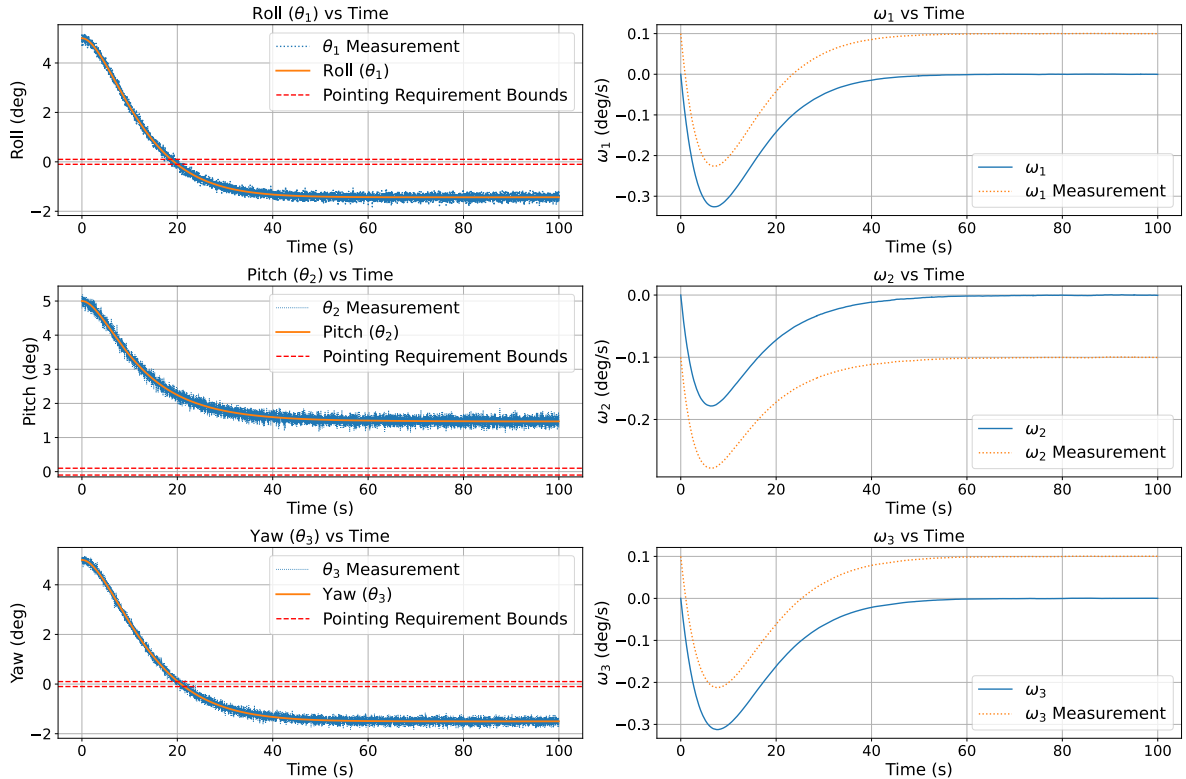


Figure 3: Attitude response using noisy attitude sensors and biased rate gyros

The introduction of realistically noisy sensor data changes the response significantly, with a steady-state error in attitude angles far outside the pointing requirement bounds of the system. The level of discrepancy in the steady-state error can be changed by adjusting the controller gains, but it cannot be entirely eliminated without switching to a more complex controller. This is because the bias in the gyro measurements will lead to a nonzero $K_d\omega$ term in the control action, which will force theta to compensate with a nonzero $K_p\theta$ term at steady-state where $M_c = 0$. Ultimately, if the spacecraft has noisy sensors and no method of state estimation, it will not be able to complete its mission within the required bounds.

State Estimator Design and Simulation

Due to the nonlinearities of the system, the Extended Kalman Filter(EKF) is chosen for state estimation. The EKF estimates the full state vector including the gyro bias, enabling the controller to operate on more accurate values. Thus, the new estimated state vector is $\hat{x} = [\hat{\theta}_1, \hat{\theta}_2, \hat{\theta}_3, \hat{\omega}_1, \hat{\omega}_2, \hat{\omega}_3, \hat{b}_1, \hat{b}_2, \hat{b}_3]^T$

EKF Variable and Matrix Definitions

The EKF requires both the Jacobian of $f(x)$, $F(x)$, and the Jacobian of the observation function $h(x)$, $H(x)$. The Jacobian function F starts from the dynamics of the new state:

$$\dot{x}_{ext} = \begin{bmatrix} \dot{\theta}_1 \\ \dot{\theta}_2 \\ \dot{\theta}_3 \\ \dot{\omega}_1 \\ \dot{\omega}_2 \\ \dot{\omega}_3 \\ b_1 \\ b_2 \\ b_3 \end{bmatrix} = \begin{bmatrix} \omega_1 + (\omega_2 \sin \theta_1 + \omega_3 \cos \theta_1) \tan \theta_2 \\ \omega_2 \cos \theta_1 - \omega_3 \sin \theta_1 \\ \frac{\omega_2 \sin \theta_1 + \omega_3 \cos \theta_1}{\cos \theta_2} \\ \frac{M_{a_1} + M_{d_1} - (J_{33} - J_{22}) \omega_2 \omega_3 - 3n(J_{33} - J_{22}) \cos \theta_1 \sin \theta_1 \cos^2 \theta_2}{J_{33}} \\ \frac{M_{a_2} + M_{d_2} - (J_{11} - J_{33}) \omega_1 \omega_3 - 3n(J_{33} - J_{11}) \cos \theta_1 \cos \theta_2 \sin \theta_2}{J_{22}} \\ \frac{M_{a_3} + M_{d_3} - (J_{22} - J_{11}) \omega_1 \omega_2 + 3n(J_{11} - J_{22}) \sin \theta_1 \sin \theta_2 \cos \theta_2}{J_{33}} \\ 0 \\ 0 \\ 0 \end{bmatrix}$$

since the gyro bias is assumed to be constant. The Jacobian then takes the form:

$$F = \begin{bmatrix} \frac{\partial f_1}{\partial \theta_1} & \frac{\partial f_1}{\partial \theta_2} & 0 & \frac{\partial f_1}{\partial \omega_1} & \frac{\partial f_1}{\partial \omega_2} & \frac{\partial f_1}{\partial \omega_3} & 0 & 0 & 0 \\ \frac{\partial f_2}{\partial \theta_1} & 0 & 0 & 0 & \frac{\partial f_2}{\partial \omega_2} & \frac{\partial f_2}{\partial \omega_3} & 0 & 0 & 0 \\ \frac{\partial f_3}{\partial \theta_1} & \frac{\partial f_3}{\partial \theta_2} & 0 & 0 & \frac{\partial f_3}{\partial \omega_2} & \frac{\partial f_3}{\partial \omega_3} & 0 & 0 & 0 \\ \frac{\partial f_4}{\partial \theta_1} & \frac{\partial f_4}{\partial \theta_2} & 0 & 0 & \frac{\partial f_4}{\partial \omega_2} & \frac{\partial f_4}{\partial \omega_3} & 0 & 0 & 0 \\ \frac{\partial f_5}{\partial \theta_1} & \frac{\partial f_5}{\partial \theta_2} & 0 & \frac{\partial f_5}{\partial \omega_1} & 0 & \frac{\partial f_5}{\partial \omega_3} & 0 & 0 & 0 \\ \frac{\partial f_6}{\partial \theta_1} & \frac{\partial f_6}{\partial \theta_2} & 0 & \frac{\partial f_6}{\partial \omega_1} & \frac{\partial f_6}{\partial \omega_2} & 0 & 0 & 0 & 0 \\ 0 & 0 & 0 & 0 & 0 & 0 & 0 & 0 & 0 \\ 0 & 0 & 0 & 0 & 0 & 0 & 0 & 0 & 0 \\ 0 & 0 & 0 & 0 & 0 & 0 & 0 & 0 & 0 \end{bmatrix}$$

for the expressions:

$$\frac{\partial f_1}{\partial \theta_1} = \omega_2 \cos \theta_1 \tan \theta_2 - \omega_3 \sin \theta_1 \tan \theta_2,$$

$$\frac{\partial f_1}{\partial \theta_2} = (\omega_2 \sin \theta_1 + \omega_3 \cos \theta_1)(\sec \theta_2)^2, \quad \frac{\partial f_1}{\partial \omega_1} = 1, \quad \frac{\partial f_1}{\partial \omega_2} = \sin \theta_1 \tan \theta_2, \quad \frac{\partial f_1}{\partial \omega_3} = \cos \theta_1 \tan \theta_2,$$

$$\frac{\partial f_2}{\partial \theta_1} = -\omega_2 \sin(\theta_1) - \omega_3 \cos(\theta_1), \quad \frac{\partial f_2}{\partial \omega_2} = \cos(\theta_1), \quad \frac{\partial f_2}{\partial \omega_3} = -\sin(\theta_1),$$

$$\frac{\partial f_3}{\partial \theta_1} = (\omega_2 \cos(\theta_1)) / \cos(\theta_2), \quad \frac{\partial f_3}{\partial \theta_2} = (\omega_2 \cos(\theta_1) - \omega_3 \sin(\theta_1)) \tan(\theta_2) (1 / \cos(\theta_2)),$$

$$\frac{\partial f_3}{\partial \omega_2} = \frac{\cos(\theta_1)}{\cos(\theta_2)}, \quad \frac{\partial f_3}{\partial \omega_3} = \frac{-\sin(\theta_1)}{\cos(\theta_2)},$$

$$\frac{\partial f_4}{\partial \theta_1} = \frac{-3n(J_{33} - J_{22})}{J_{11}} \cos 2\theta_1 (\cos \theta_2)^2, \quad \frac{\partial f_4}{\partial \theta_2} = \frac{-3n(J_{33} - J_{22})}{J_{11}} \cos(\theta_1) \sin(\theta_1) (-\sin 2\theta_2),$$

$$\begin{aligned}
\frac{\partial f_4}{\partial \omega_2} &= \frac{-(J33 - J22)\omega_3}{J11}, & \frac{\partial f_4}{\partial \omega_3} &= \frac{-(J33 - J22)\omega_2}{J11}, \\
\frac{\partial f_5}{\partial \theta_1} &= \frac{-3n(J33 - J11)}{J22} \sin(\theta_1) \cos(\theta_2) \sin(\theta_2), & \frac{\partial f_5}{\partial \theta_2} &= \frac{3n(J33 - J11)}{J22} \cos(\theta_1) \cos(2\theta_2), \\
\frac{\partial f_5}{\partial \omega_1} &= \frac{-(J11 - J33)}{J22} \omega_3, & \frac{\partial f_5}{\partial \omega_3} &= \frac{-(J11 - J33)}{J22} \omega_1, \\
\frac{\partial f_6}{\partial \theta_1} &= \frac{3n(J11 - J22)}{J33} \cos(\theta_1) \sin(\theta_2) \cos(\theta_2), & \frac{\partial f_6}{\partial \theta_2} &= \frac{3n(J11 - J22)}{J33} \sin(\theta_1) \cos(2\theta_2), \\
\frac{\partial f_6}{\partial \omega_1} &= \frac{-(J22 - J11)}{J33} \omega_2, & \frac{\partial f_6}{\partial \omega_2} &= \frac{-(J22 - J11)}{J33} \omega_1,
\end{aligned}$$

The Jacobian of the observation matrix is much simpler, as taking the Jacobian of $h(x)$ in Equation 1 yields:

$$H = \begin{bmatrix} 1 & 0 & 0 & 0 & 0 & 0 & 0 & 0 & 0 \\ 0 & 1 & 0 & 0 & 0 & 0 & 0 & 0 & 0 \\ 0 & 0 & 1 & 0 & 0 & 0 & 0 & 0 & 0 \\ 0 & 0 & 0 & 1 & 0 & 0 & 1 & 0 & 0 \\ 0 & 0 & 0 & 0 & 1 & 0 & 0 & 1 & 0 \\ 0 & 0 & 0 & 0 & 0 & 1 & 0 & 0 & 1 \end{bmatrix}$$

The next step in designing the EKF is creating the error covariance matrices Q, R, and P. The process noise covariance matrix Q represents the uncertainty in the dynamics themselves. Generally, for a well-defined process in space, there will be few noise contributions to the system itself other than small gravitational, magnetic, or solar disturbances. As such, Q will be a diagonal matrix with very small values on the diagonal. For the examined case, the continuous-time Q matrix is defined as:

$$Q_{ct} = \text{diag}(0, 0, 0, 10^{-8}, 10^{-8}, 10^{-8}, 10^{-10}, 10^{-10}, 10^{-10})$$

The continuous-time Q matrix is scaled by Δt following the equation $Q = Q_{ct} \cdot \Delta t$ to turn it into the discrete-time Q used in the EKF.

The measurement noise covariance matrix R represents, as the name suggests, the uncertainty in measurement caused by noise processes in sensors. Generally, R is a diagonal matrix with the variances on the diagonal, which for this system would lead to:

$$R = \text{diag}(\sigma_{\theta_1}^2, \sigma_{\theta_2}^2, \sigma_{\theta_3}^2, \sigma_{\omega_1}^2, \sigma_{\omega_2}^2, \sigma_{\omega_3}^2)$$

It is often suggested to replace zeros in the R matrix with very small numbers for numerical stability in the EKF, so the σ_ω^2 values are all 10^{-8} .

Finally, the state estimation error covariance matrix P represents the uncertainty of the EKF's estimate for the state at each timestep. P is updated every timestep, so it is normally expressed as $P_{i|j}$, or the covariance of the prediction for state at step i that was made at step j.

EKF Steps

The EKF is broken into two steps: Predict and Update.

The predict step is, as the name suggests, simply predicting the \hat{x} values and P matrix for the next step based on the \hat{x} and P for the previous step. In order to predict the next state, one can use Euler integration via the formula:

$$x_{k,pred} = \hat{x}_{k-1} + f(x, u)\Delta t \quad (2)$$

To predict the P matrix, the process is slightly more involved. First, the continuous-time dynamics have to be converted to discrete-time dynamics using the equation

$$\Phi_k = e^{F(x_k)} \quad (3)$$

Where $F(x_k)$ is the Jacobian of the system dynamics $\dot{x} = f(x, u)$ evaluated at x_k . Once Φ is obtained, the predicted P for step k can be found using the equation:

$$P_{k,pred} = \Phi P_{k-1} \Phi^T + Q \quad (4)$$

The update step takes in $x_{k,pred}$ and $P_{k,pred}$ to and combines them to get the final \hat{x}_k and P_k for the timestep. In order to get these values, the Kalman gain matrix K must be found for the timestep using the equation:

$$K_k = P_{k,pred} H^T (H P_{k,pred} H^T + R)^{-1} \quad (5)$$

Then, the full estimation for the state x, \hat{x}_k and estimate covariance P_k a step k can be found via the equations:

$$\hat{x}_k = x_{k,pred} + K_k (x_{k,meas} - h(x_{k,pred})) \quad (6)$$

$$P_k = (I - KH) P_{k,pred} \quad (7)$$

Where $h(x_{k,pred})$ is the observation equation used in Equation 1 evaluated at the estimated angles, angular rates, and biases, and H is the Jacobian of the observation equation. This process is repeated at each timestep to continually predict the state of the system and the covariance of the estimate.

EKF Initialization

The state and the P matrix must be initialized to use the EKF. For initializing P, the standard deviation of the attitude angle noise was used for all θ values, 10^{-6} was used for all ω values, and 10^{-2} was used for all biases. The final expression was therefore:

$$P_{0,est} = \text{diag}([\sigma_{w_1}^2, \sigma_{w_2}^2, \sigma_{w_3}^2, (1e-3)^2, (1e-3)^2, (1e-3)^2, (0.1)^2, (0.1)^2, (0.1)^2])$$

These initializing numbers are somewhat flexible, as they should converge to stable values as the system is simulated. The estimated state \hat{x} , is initialized to the true initial values of the system: $\theta_1 = \theta_2 = \theta_3 = 5^\circ$ and $\omega_1 = \omega_2 = \omega_3 = b_1 = b_2 = b_3 = 0$.

Integration into Controls

The same PD controller was used in the EKF case, with one minor difference being how the omega gain was applied. Previously, the controller applied was defined as:

$$M_c = K_p \bar{\theta}_{meas} + K_d \bar{\omega}_{meas}$$

Now, to account for the predicted biases, the new control action is defined as:

$$M_c = K_p \bar{\theta}_{meas} + K_d (\bar{\omega}_{meas} - \hat{b})$$

Where \hat{b} is the vector of predicted biases for the gyroscopes.

Simulation Results

Using the EKF, the system was simulated and the estimated state was plotted alongside the true state. The results can be seen in Figure 4 with estimated states in orange and actual states in blue.

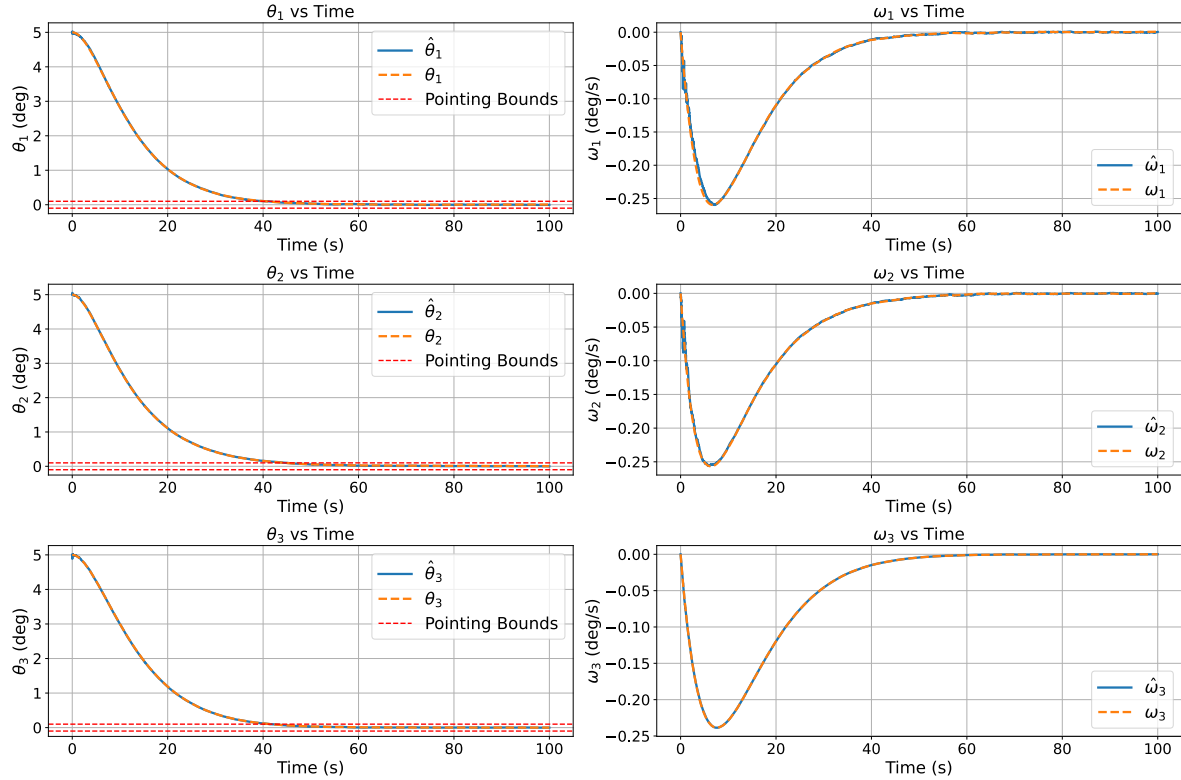


Figure 4: Attitude and Rate Response with EKF Included in Control Loop

The addition of the EKF leads to a significant improvement in tracking accuracy, and the estimated state is very close to the actual state for almost all times of all graphs. The line representing the estimated attitude and the actual attitude are almost indistinguishable at most times, even while one is plotted in blue and the other is plotted in orange. In addition, the system response requirements are met for roll, pitch, and yaw.

Bias Estimation

Figure 5 shows the bias estimate as a function of time for b_1 , b_2 , and b_3 :

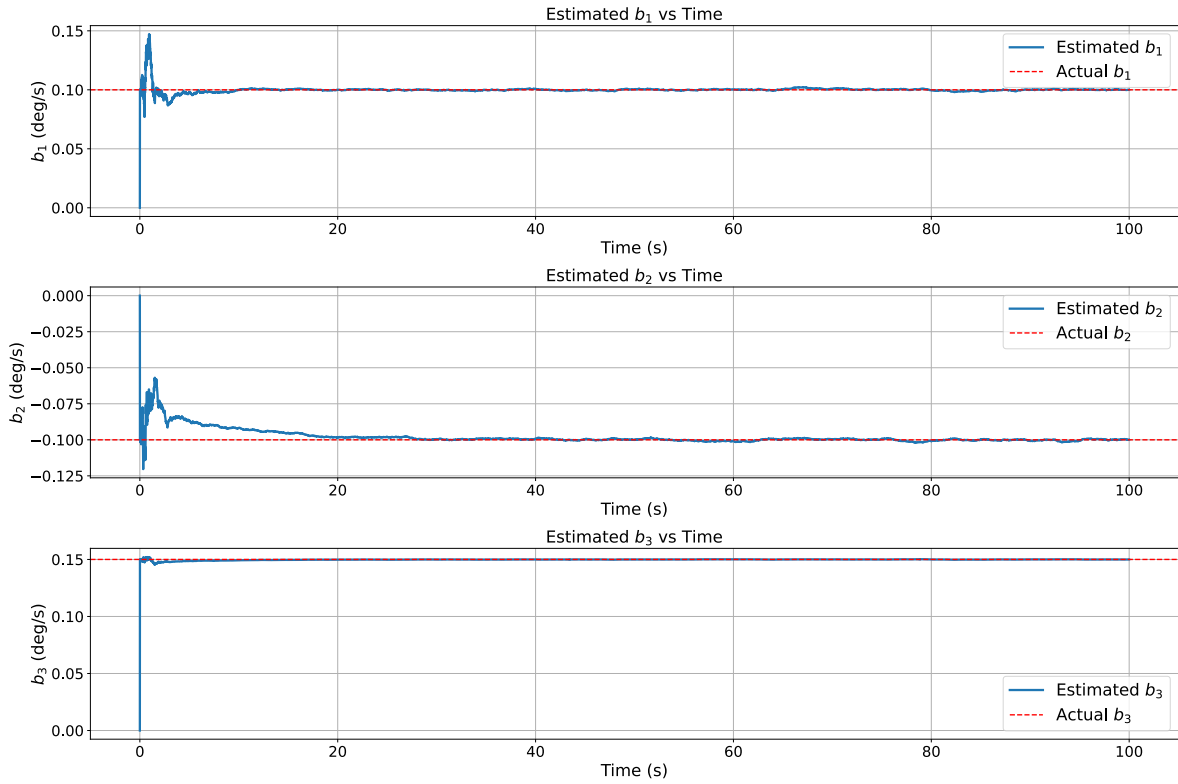


Figure 5: Gyroscope Bias Estimation Over Time

The bias estimates converge on the actual bias value within 20 seconds, which mitigates the steady-state error seen in the non-EKF simulation with noise.

EKF Statistical Analysis

To evaluate the EKF across a range of initial estimates, the noisy system with the EKF was simulated ten times; five with an initial estimated attitude as the actual attitude, and five with the initial estimated attitude as 0. For each simulation, the average difference between the actual θ , ω and b and the estimated $\hat{\theta}$, $\hat{\omega}$ and \hat{b} were found and labeled as $\Delta\theta$, $\Delta\omega$, and Δb . Across all runs of the same initial condition, the mean and standard deviation of the differences were also found. The results can be seen in Tables 2 and 3:

Table 2: EKF Performance with Correct Initial Attitude

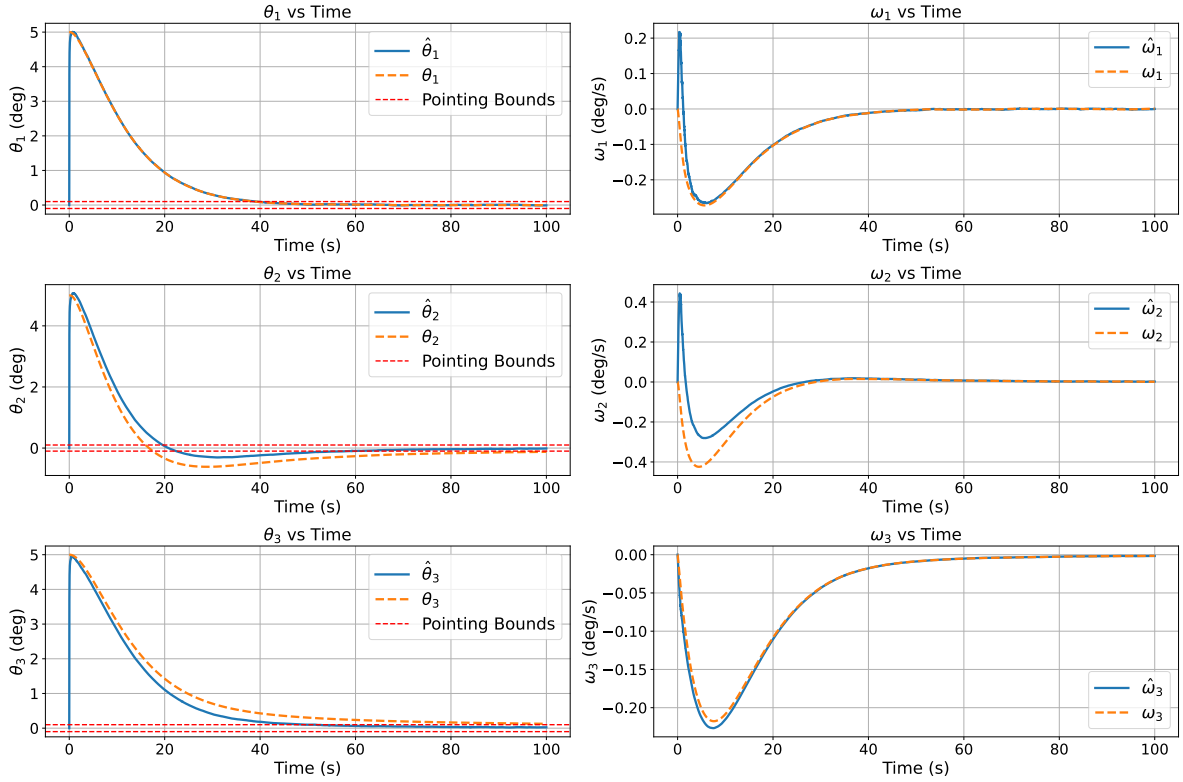
Run	Avg. $\Delta\theta$ [deg]	Avg. $\Delta\omega$ [deg/s]	Avg. Δb [deg/s]
1	0.004107	0.000708	0.000719
2	0.004342	0.000705	0.000716
3	0.003884	0.000611	0.000622
4	0.018211	0.001482	0.001494
5	0.003591	0.000595	0.000606
Mean	0.006827	0.000820	0.000831
Std Dev	0.006306	0.000365	0.000362

Table 3: EKF Performance with Initial Attitude at Zero

Run	Avg. $\Delta\theta$ (deg)	Avg. $\Delta\omega$ (deg/s)	Avg. Δ Bias (deg/s)
Run 1	0.140603	0.010894	0.009616
Run 2	0.144190	0.011091	0.009721
Run 3	0.148842	0.011477	0.009953
Run 4	0.134247	0.010410	0.009066
Run 5	0.139283	0.010805	0.085556
Mean	0.141433	0.010935	0.024782
Std. Dev.	0.005364	0.000389	0.033541

As Table 1 shows, the average difference between actual and estimated θ , ω , and b are very small in the case where the EKF is initialized at the actual attitude angles. The average $\Delta\theta$ at 0.006827° is about 6.8% of the standard deviation of the measurement noise. It is important to note that the standard deviation of the average $\Delta\theta$ is 92% of the mean value, so there is significant variation in the average difference depending on the run. Bias estimation differences are also very low, with the highest bias in any individual run at $0.000831^\circ/s$, which is about 0.5% of the max bias in the system.

On the other hand, Table 3 shows an important characteristic of the EKF, which is that the initialization is critical for its effective use. When the system is initialized at $\hat{x} = 0$, the $\Delta\theta$, $\Delta\omega$, and Δb are respectively 2000%, 1330%, 2980% higher than the cases where the system is initialized at $\hat{x} = x_{actual}$. This means that the average difference between estimated and actual value is higher than the system pointing requirements. This discrepancy can be seen when plotting the spacecraft's time response when the EKF is initialized at zero, as in Figure 6:

**Figure 6:** Attitude and Rate Response with EKF Initialized at $\hat{x} = 0$

The average is slightly skewed by the first half of the system taking time to adjust, but it is an important consideration for a system with strict attitude control requirements.

Performance Comparison

To more easily compare the three cases, a unified plot was created to directly compare the ideal sensor case, the noisy sensor case with no EKF, and the noisy sensor case with the EKF as a state estimator(initialized at actual state). This can be seen in Figure 7:

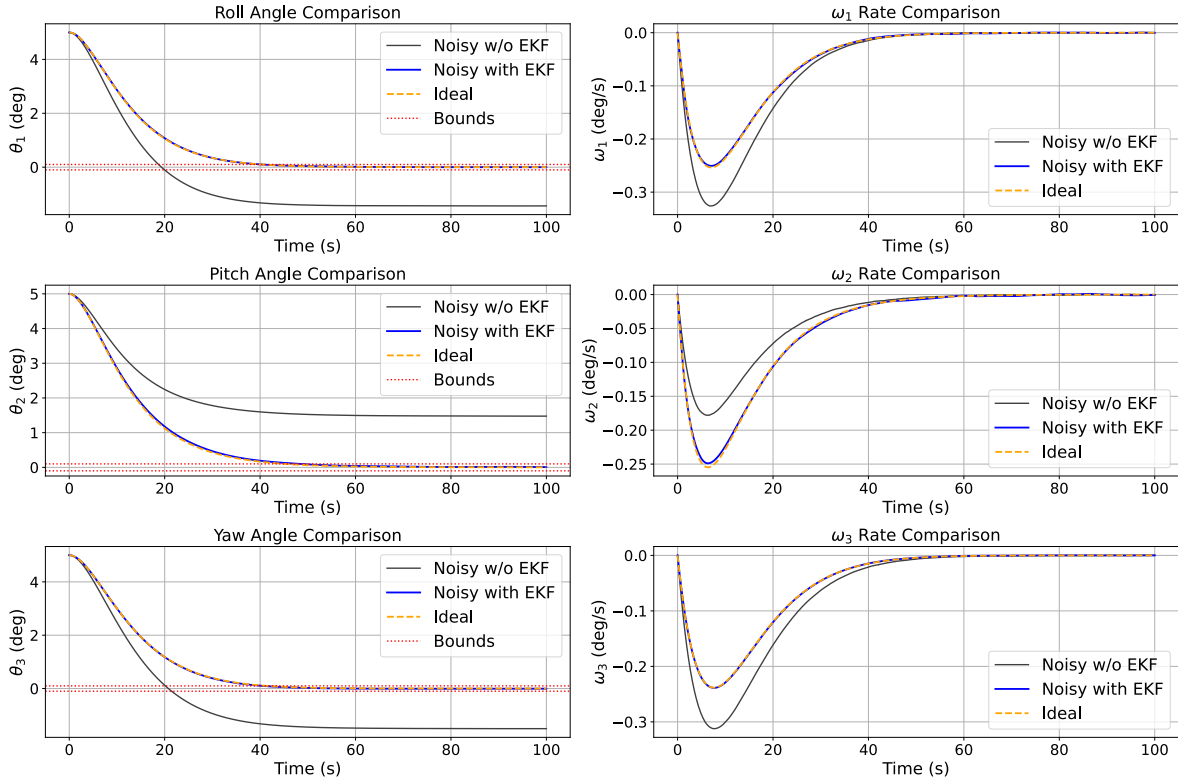


Figure 7: Comparison of attitude tracking with ideal sensors, noisy sensors, and EKF-based estimation

The comparison confirms the expected belief that adding noise and bias to the sensor stack leads to a steady-state error in the final attitude angle due to the bias term inducing an equalizing response from the θ term in the control equation. On the other hand, when the EKF is included, the spacecraft attitude follows very closely with the attitude in the case where there are ideal sensors, maintaining the $\pm 0.1^\circ$ bounds on pointing accuracy.

Conclusion

This report displays how powerful the EKF is as a tool for state estimation and, as a downstream effect, control of a spacecraft with strict mission parameters. The EKF proved to improve the performance of the noisy system such that it almost resembled the case with ideal sensors. It eliminates the steady-state error associated with the gyro bias via its fast-converging and accurate bias estimation. Overall, it shows how a relatively simple algorithm, the Kalman Filter, can be extended to nonlinear systems in order to increase their performance significantly and cheaply, since it allows the use of flawed sensors instead of incredibly expensive and incredibly precise sensors. One important caveat is that the initialization of the EKF must be done precisely in order to get the best results from the algorithm, as inaccuracies at initialization can compound into lingering inaccuracies of the system.

Bibliography

Van Kampen, E. (2025). *Lecture 3: Vehicle Dynamics*. TU Delft Aerospace Engineering.

Van Kampen, E. (2025). *Lecture 4: State Estimation*. TU Delft Aerospace Engineering.